Journal of Solid State Chemistry 240 (2016) 16–22

Contents lists available at ScienceDirect

Journal of Solid State Chemistry

journal homepage: www.elsevier.com/locate/jssc

Relationship between ferroelectric properties and local structure of $Pb_{1-x}Ba_xZr_{0.40}Ti_{0.60}O_3$ ceramic materials studied by X-ray absorption and Raman spectroscopies

Alexandre Mesquita [a,b,d,*], Alain Michalowicz [b], Jacques Moscovici [b], Paulo Sergio Pizani [c], Valmor Roberto Mastelaro [d]

[a] Instituto de Geociências e Ciências Exatas, UNESP – Univ Estadual Paulista, Departamento de Física, Av. 24-a, 1515, Rio Claro, SP 13506-900, Brazil
[b] Institut de Chimie et des Materiaux Paris Est, CNRS and Université Paris Est Créteil, 2 Rue Henri Dunant, 94320 Thiais, France
[c] Departamento de Física, Universidade Federal de São Carlos, Rodovia Washington Luís, s/n, São Carlos, SP, 13565-905, Brazil
[d] Instituto de Física de São Carlos, Universidade de São Paulo, Av. Trabalhador São-Carlense, 400, São Carlos, SP, Brazil

ARTICLE INFO

Article history:
Received 2 March 2016
Received in revised form
10 May 2016
Accepted 11 May 2016
Available online 13 May 2016

Keywords:
Ferroelectrics
Relaxor, PBZT
PZT, EXAFS
Raman

ABSTRACT

This paper reports on the structural characterization of $Pb_{1-x}Ba_xZr_{0.40}Ti_{0.60}O_3$ (PBZT) ferroelectric ceramic compositions prepared by the conventional solid state reaction method. X-ray absorption spectroscopy (XAS) and Raman spectroscopy were used in the probing of the local structure of PBZT samples that exhibit a normal or relaxor ferroelectric behavior. They showed a considerable local disorder around Zr and Pb atoms in the samples of tetragonal or cubic long-range order symmetry. The intensity of the *E(TO$_3$)* mode in the Raman spectra of PBZT relaxor samples remains constant at temperatures lower than T_m, which has proven the stabilization of the correlation process between nanodomains.

1. Introduction

Lead zirconate titanate ($PbZr_{1-y}Ti_yO_3$), also referred to as PZT ceramic system, has been extensively studied due to its unique properties that enable a wide variety of applications in piezoelectric, pyroelectric and ferroelectric devices [1,2]. The PZT system exhibits a cubic structure at higher temperatures and three different structures at room temperature, depending on the composition, which can be tetragonal, orthorhombic or rhombohedral. According to the proposed phase diagram, all compositions are tetragonal and exhibit a *P4mm* symmetry on the titanium-rich side [2]. On the other hand, depending on *y* value and the temperature, two rhombohedral phases, *R3m*, often referred to as FR (HT), and *R3c*, referred to as FR(LT), occur in Zr-rich PZT ceramics [3]. The region between tetragonal and rhombohedral phases ($y \sim 0.50$) is called morphotropic phase boundary (MPB) and characterized by the presence of those two phases and monoclinic symmetry with *Cm* space group, which is a subgroup of *P4mm* and *R3m* space groups [4]. For all values of *y*, the PZT system exhibits a long-range ferroelectric order, micrometer domain and/or domain wall structures and shows no frequency dispersion (relaxational effect) in the audio frequency range [5].

However, pure PZT ceramic materials are rarely applied to electronic devices and a doping process enhances their properties [2,6]. For example, La^{3+} cations have substituted the Pb^{2+} cations and formed a $Pb_{1-x}La_xZr_{1-y}Ti_yO_3$ (PLZT) system. This substitution induces a peculiar diffuse phase transition with frequency dispersion and both La^{3+} aliovalent ions and/or oxygen vacancies, necessary to preserve charge neutrality, are believed to break the translational symmetry of the lattice and represent a type of disorder responsible for the formation of polar nanodomains, hence, a relaxor feature [5].

The substitution of Pb^{2+} by Ba^{2+} cations that form the $Pb_{1-x}Ba_xZr_{1-y}Ti_yO_3$ (PBZT) system has been also studied in details. Since the publication of the PBZT phase diagram [7], several studies have been conducted due to its variety of interesting physical properties of technological and fundamental importance and the relaxor ferroelectric behavior exhibited by certain PBZT compositions [5,8]. In comparison with PZT samples containing lanthanum, a higher amount of barium is required for the occurrence of a relaxor behavior [5,9]. Although this difference has not been completely understood, it has been related to vacancies created by the heterovalent substitution of Pb^{2+} by La^{3+}. The high amount of

* Corresponding author at: Instituto de Geociências e Ciências Exatas, UNESP – Univ Estadual Paulista, Departamento de Física, Av. 24-a, 1515, Rio Claro, SP 13506-900, Brazil.
E-mail addresses: mesquita@rc.unesp.br (A. Mesquita), michalov@u-pec.fr (A. Michalowicz), moscovic@u-pec.fr (J. Moscovici), pizani@df.ufscar.br (P.S. Pizani), valmor@ifsc.usp.br (V.R. Mastelaro).

http://dx.doi.org/10.1016/j.jssc.2016.05.016
0022-4596/

Ba^{2+} in the PBZT system necessary for the occurrence of the relaxor behavior would be related to defects in the structure caused only by the difference between Pb and Ba ionic radius [5].

X-ray diffraction (XRD) results of PBZT ferroelectric relaxor materials showed the existence of a long-range order cubic symmetry with no phase transition above and below the temperature of maximum dielectric permittivity (T_m) [10,11]. However, such symmetry is not compatible with a ferroelectric relaxor state.

Short-range order structure characterization techniques, such as X-ray absorption spectroscopy (XAS) and Raman spectroscopy, have revealed the existence of a high degree of local disorder above and below T_m, which is apparently not compatible with the long-range order cubic symmetry detected by XRD [12–14]. In fact, XAS technique is a powerful tool for the investigation of local structures and provides meaningful additional structural information on materials [15]. Although the local structural data afforded by XAS are usually not sufficient for the construction of a whole structural model, they often provide valuable information about the local structural peculiarities [16]. Pair distribution function analysis (PDF) is also able to give valuable local information [17]. However, we have decided to complete our preceding studies with the same synchrotron structural tool, EXAFS.

Pb atoms are of particular importance in PZT-based systems, as they hybridize with oxygen states, which leads to a large off-center displacement for the B atoms in the ABO_3 structure, hence, a high polarization and ferroelectric order [18,19]. Recent studies have also shown the importance of the B atom site displacement in the BO_6 octahedron in the normal-to-relaxor ferroelectric transition [20–22]. Larger B atom off-center displacements cause the overbonding of oxygen atoms to be alleviated by the motion of B atoms away from the O atom, which leads to the stabilization of the normal ferroelectric phase [21]. The Zr displacement will produce a small Zr polarization that can be aligned with a modest electric field and create a favorable energetic situation for the switching of the strongly polar Ti–O dipole [18]. Therefore, a Zr shift can also play an important role for the large ferroelectric order in PZT-based systems.

We have carefully studied the local and electronic structure around Ti atoms in Ti-rich PBZT samples by X-ray absorption near edge structure (XANES) and observed a large Ti off-centering displacement as a function of Ba content in PBZT samples, even for the samples characterized as cubic by XRD Rietveld refinement and as relaxors from dielectric measurements [23].

Due to the important role played by Pb and Zr atoms in the normal to relaxor ferroelectric phase transition and to complete our previous structural study of PBZT ferroelectric ceramics, in which only the short-range order around Ti atoms was characterized, we present a short-range order analysis for Pb^{2+} and Zr^{4+} atoms. To the best of our knowledge, Zr and Pb short-range order in a Ti-rich PBZT system has not been characterized by XAS and Raman spectroscopy techniques.

2. Experimental procedure and methods of data analysis

$Pb_{1-x}Ba_xZr_{0.40}Ti_{0.60}O_3$ samples (denoted as PBZT100x) with x=0.00 (PZT), 0.10, 0.20, 0.30, 0.40 and 0.50 at% of Ba were prepared by the conventional mixed oxide method and conventional sintering route. Details are provided elsewhere [24].

Pb L_{III}-edge (13,055 eV) Extended X-ray Absorption Fine Structure (EXAFS) spectra were collected in transmission mode at the D04B-XAS2 beamline of the Brazilian National Synchrotron Light Laboratory (LNLS). Zr K-edge EXAFS and X-ray Absorption Near Edge Spectroscopy (XANES) spectra were collected on the SAMBA beamline at SOLEIL, the French Synchrotron facility. All the XAFS data were collected at room temperature. The thicknesses of the samples were optimized at each edge by the Multi-Platform Applications for XAFS (MAX) software package Absorbix code [25]. XANES and EXAFS spectra were normalized by the MAX-Cherokee code, whereas the MAX-Roundmidnight package was used for the fitting procedure and comparison between experimental and theoretical EXAFS curves. The theoretical EXAFS spectra with Pb substituted by Ba were calculated by the FEFF8 code [26]. The fitting quality was analyzed according to the recommendations of IXS standard and criteria reports and the relevant measure of the fit quality, i.e., reduced statistical χ^2, named QF (quality factor) [27].

Raman scattering measurements were performed by a Coherent INNOVA 70 C Spectrum laser and a Jobin-Yvon T64000 triple monochromator with a charge-coupled device detector. The 514 nm line of an argon laser was used as the exciting light and its power was kept below 1 mW. Raman spectra were collected by a 50-time magnifying lens objective. All Raman spectra were normalized by population factor.

3. Results and discussion

The XANES and EXAFS spectra at the Zr K-edge were collected at room temperature for PZT ($PbZr_{0.40}Ti_{0.60}O_3$, x=0, normal ferroelectric), PBZT20 ($Pb_{0.80}Ba_{0.20}Zr_{0.40}Ti_{0.60}O_3$, x=0.20, normal ferroelectric) and PBZT40 ($Pb_{0.60}Ba_{0.40}Zr_{0.40}Ti_{0.60}O_3$, x=0.40, relaxor ferroelectric) samples. All Zr EXAFS spectra were cut at k=12 $Å^{-1}$ due to the presence of an important and unrecoverable glitch just above this value.

Fig. 1 shows the normalized Zr K-edge XANES spectra of PZT, PLZT20 and PLZT40 samples and $BaZrO_3$ as the reference compound. The three spectra are almost identical, which shows the Zr environment was not significantly affected by the substitution of Pb^{2+} by Ba^{2+}. The Zr K-pre-edge region related to 1s to 4d+5p states transition is more pronounced in Zr off-centering structures [28]. The two peaks between 18,017 and 18,035 eV are related to 1s to 5p states transition of Zr atoms in an octahedral symmetry [28,29]. Unlike the Ti edge, the Zr pre-edge transition appears as a shoulder under the main edge, therefore, its amplitude cannot be used as a quantitative signature of the Zr off-center displacement.

An EXAFS study was conducted at the Zr K-edge for more quantitative structural information about the Zr local order. Fig. 2 (a) shows the Zr K-edge Fourier transform (FT) moduli of PZT,

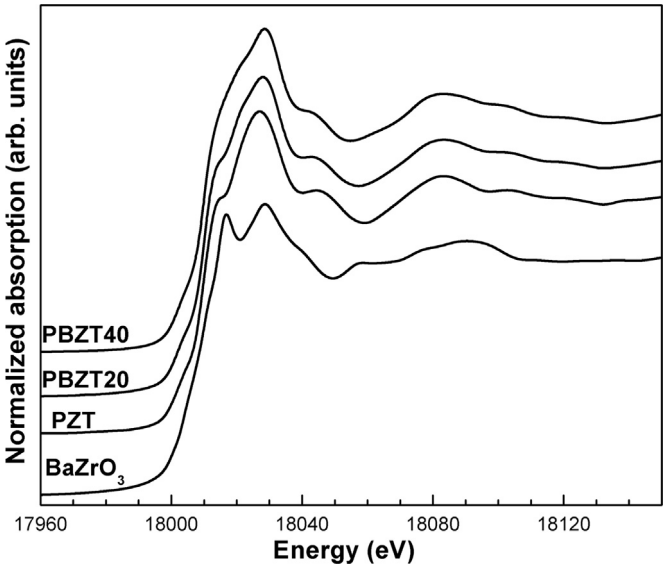

Fig. 1. Zr K edge XANES spectra of PZT, PBZT20 and PBZT40.

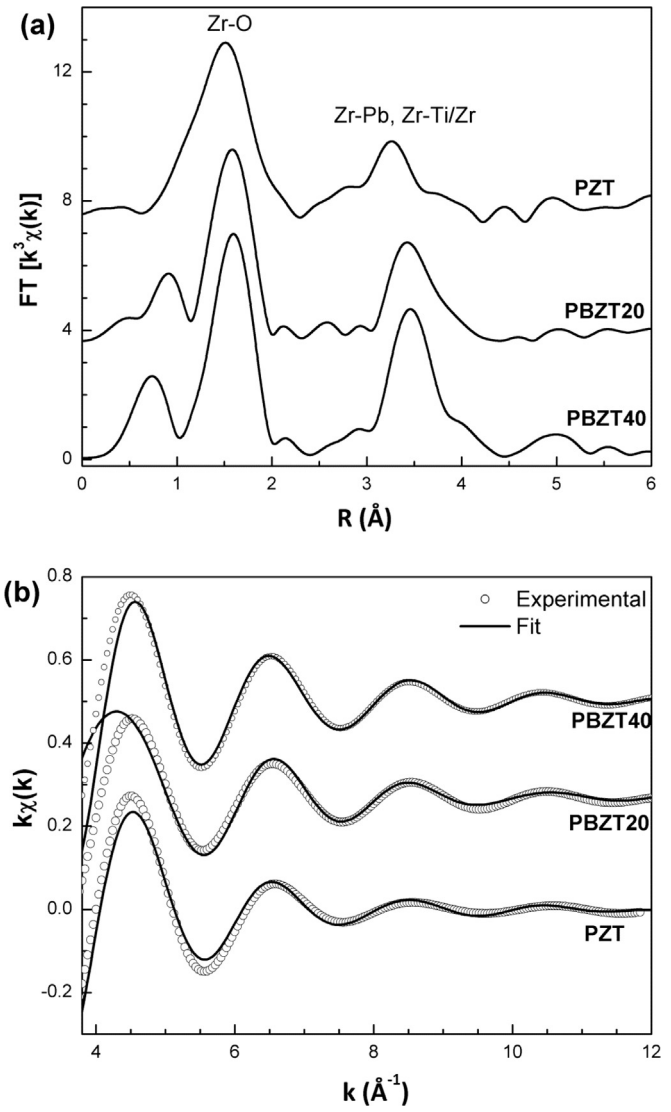

Fig. 2. (a) Modulus of the Fourier transforms of $k^3\chi(k)$ Zr K-edge spectra for PZT, PBZT20 and PBZT40 samples and (b) experimental and fitted back-Fourier-filtered for the same samples.

PBZT20 and PBZT40 samples. The first intense FT peak is related to the Zr–O distances on the ZrO_6 octahedral site, whereas the peaks beyond the first neighbors ($R > 2.5$ Å) represent single scattering paths relative to Zr–Pb/Ba, Zr–Ti/Zr and Zr–O and multiple scattering paths, such as Zr–O–O, Zr–O–Zr, Zr–O–Zr–O, Zr–O–Pb, Zr–Ti–O and Zr–O–Ti–O. Due to the complexity of the components and the noise level, we focused the Zr local order quantitative study on the first FT peak.

Initially, the EXAFS spectra were fitted according to a local tetragonal symmetry model based on the XRD results from the Rietveld analysis with different sets (coordination shells) of Zr–O mean bond-lengths [24]. Each shell can be represented by four fitted parameters, namely number of neighbors (N), Debye-Waller factor (DW), representing the local disorder (σ^2), central atom-neighbour distance (R) and shift of the energy origin ΔE_0. However, the number of parameters (N_{par}) must be minimized for the avoidance of fitting drawbacks due to the poor statistics of the data (number of independent points, $N_{ind} = 13$) on the parameters correlations. Therefore, the total number of oxygen neighbors was fixed to 6 and the Debye Waller factor was considered the same for all shells. The energy threshold ΔE_0 adjustment was also constrained to a unique value, since the use of different energies may lead to unphysical results [30,31]. Table 1 shows the best fitting results for each sample defined by the minimum value of QF. Fig. 2 (b) shows the experimental and fitted Fourier-filtered contributions from *r*-space between ~1.0 and 2.5 Å.

Table 1
Interatomic distances (R), Debye-Waller factor (σ^2) and quality factor (QF) of PZT, PBZT20 and PBZT40 samples obtained through Zr K-edge filtered first shell EXAFS fitting.

Sample	Shell	*R* (Å)	σ^2 (Å^2)	QF
PZT	1 Zr–O_I	1.78(2)	0.010(1)	1.23
	4 Zr–O_{II}	2.04(1)		
	1 Zr–O_{III}	2.61(4)		
PBZT20	1 Zr–O_I	1.81(5)	0.008(2)	1.55
	4 Zr–O_{II}	2.01(2)		
	1 Zr–O_{III}	2.50(7)		
PBZT40	1 Zr–O_I	1.75(3)	0.007(2)	1.34
	4 Zr–O_{II}	2.09(4)		
	1 Zr–O_{III}	2.29(9)		

The Zr off-center displacement $\Delta R = (R_{long} - R_{short})/2$ was calculated by the mean bond distances obtained from the EXAFS fitting and compared with the one obtained from previous XRD data [24]. As shown in Table 2, the ZrO_6 octahedron site distortion probed by EXAFS remains important and does not follow the crystallographic transition from a local tetragonal site symmetry for PZT to a cubic local structure for PBZT50 [24]. This result is similar to the one from the analysis of Ti K-edge XANES spectra [23].

According to Cao et al. [32], the displacement of Zr atoms from the centrosymmetric position in the $PbZr_{1-x}Ti_xO_3$ sample obtained from Zr K-edge EXAFS measurements is approximately 0.07 Å. A Zr off-center displacement around 0.1–0.3 Å was also obtained from density functional theory calculations for the $PbZr_{0.50}Ti_{0.50}O_3$ composition [33,34].

The analysis of Zr and Ti off-center displacement has been considered one of the keys for a better understanding of the dielectric properties of PZT and PBZT samples. Unfortunately, despite the structural data available in the literature, the discussion remains confusing, especially when XRD and XAS results are compared. The apparent disagreement between XRD and XAS data is far from being astonishing. The averaged local structure of $Pb_{1-x}Ba_xZr_{0.40}Ti_{0.60}O_3$ samples obtained from powder XRD Rietveld refinements is not accurate due to:

i) a substitutional disorder on two different sites (Pb by Ba on *A* site and Zr by Ti on *B* site) - despite their different radii, each site is constrained to be unique in the XRD refinement;
ii) a displacement disorder: the Ti and Zr off-center displacement is considered identical to limit the number of parameters, which leads to a systematic average effect; and
iii) an orientation disorder: a random substitution of Pb by Ba should influence the distortion on the Zr neighboring site. However, in the XRD refinement, the orientation of this distortion is assumed ordered.

All such structural effects lead to averaged unit cell parameters

Table 2.
Off-center displacement of Zr from ZrO_6 octahedra for PZT, PBZT20 and PBZT50 samples.

Sample	ΔR (XRD)	ΔR (EXAFS)
PZT	0.36(1) Å	0.41(4) Å
PBZT20	0.13(1) Å	0.34(9) Å
PBZT40	0.05(1) Å	0.27(9) Å

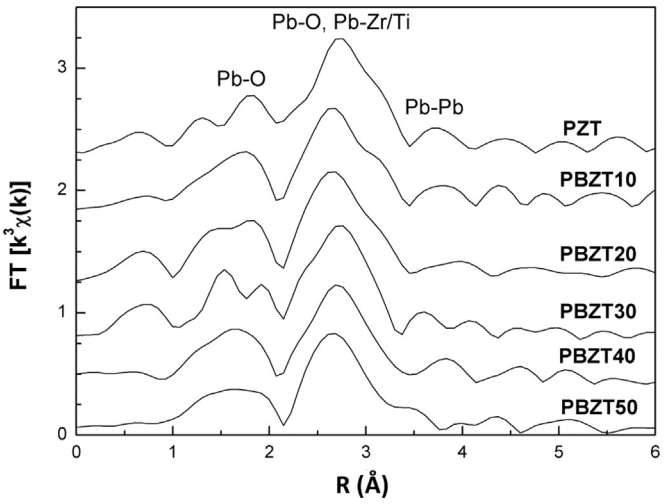

Fig. 3. Fourier transform modulus of Pb L_{III}-edge EXAFS spectra of PBZT samples at room temperature.

and atomic positions, therefore, a quantitative comparison of the local structure probed by the long-range order XRD technique and local order probed by XAS becomes unfeasible.

The moduli of Fourier transform (FT) relative to the EXAFS spectra at the Pb L_{III}-edge as a function of the Ba content are shown in Fig. 3. We can observe only a slight evolution of the FT moduli and will not consider the FT moduli peaks beyond 3.2 Å because their intensity is significantly lower.

Due to the discrepancy between XRD and XAS results of samples that exhibit a long-range order cubic structure, we focused our attention on the quantitative analysis of the Pb L_{III}-edge EXAFS spectra of the PBZT50 sample.

The experimental EXAFS spectra were fitted through theoretical models based on cubic and tetragonal local symmetries. The MAX-Roundmidnight package enables a qualitative comparison of the experimental and theoretical EXAFS spectra obtained from the FEFF8.2 code. The FEFF input files issued from MAX-Crystalffrev software were obtained with previous XRD data [24]. Multiple scattering paths identified only beyond 3.5 Å in the Fourier transform, as well as the first contributions from Pb/La shell and other Pb–O ad Pb–T/Zr shells were not considered.

According to Table 3, the local tetragonal symmetry model consists of three sets of different Pb–O distances displaced at 2.55 Å, 2.89 Å and 3.26 Å and two Pb–Ti/Zr distances at 3.40 Å and 3.63 Å. The moderate difference among the three Pb–O distances results in a significant overlap and interference effect responsible for the peaks splitting. According to the cubic symmetry local structural model depicted in Table 3, the neighborhood of Pb atoms is formed by a shell with twelve O atoms at 2.88 Å and a shell formed by five Ti atoms and three Zr atoms at 3.48 Å.

The experimental Fourier-filtered contribution obtained from the *r*-space between 1.0 and 3.5 Å of the PBZT50 FT curve was then fitted by the tetragonal and cubic models described above. The results of the fitting are provided in Table 4 and the comparison between experimental and fitted EXAFS spectra showed in Fig. 4 confirmed the better agreement with the local tetragonal model, although the PBZT50 sample was characterized by XRD as exhibiting a local cubic symmetry.

Pb L_{III}-edge EXAFS spectra of PZT and PLBT30 samples were also collected at 500 °C and 300 °C, which are above the maximum temperature of the dielectric permittivity curve (T_m) of PZT (T_m=410 °C) and PBZT30 (T_m=216 °C) samples [24]. Such samples exhibit a paraelectric behavior at 300 °C and 500 °C, respectively [24]. As shown in Fig. 5, the FT's of PZT and PBZT30 samples collected at those temperatures are characteristic of a local tetragonal

Table 3.
Tetragonal and cubic structural parameters obtained from XRD refinement and related FEFF model of PBZT50 [24].

XRD tetragonal parameters				
	a	b	c	
	4.007734	4.007734	4.149705	
	x/a	y/b	z/c	occupancy
Pb/Ba	0.0000	0.0000	0.00004	0.50/0.50
Zr/Ti	0.5000	0.5000	0.546333	0.40/0.60
O1	0.5000	0.5000	0.132456	1
O2	0.5000	0.0000	0.620271	1
FEFF tetragonal model				
Pb neighbour	amplitude ratio	degeneracy	nleg	R
Pb–O_1	100	4	2	2.55
Pb–O_2	71	4	2	2.89
Pb–O_3	50	4	2	3.26
Pb–Ti_1	39	3	2	3.40
Pb–Zr_1	14	1	2	3.40
Pb–Ti_2	22	2	2	3.63
Pb–Zr_2	24	2	2	3.63
XRD cubic structural parameters				
	a	b	c	
	4.01983	4.01983	4.01983	
	x/a	y/b	z/c	occupancy
Pb/La	0.0000	0.0000	0.0000	0.50/0.50
Zr/Ti	0.5000	0.5000	0.5000	0.40/0.60
O_1	0.5000	0.5000	0.0000	1
O_2	0.5000	0.0000	0.5000	1
FEFF cubic model				
Pb neighbour	amplitude ratio	degeneracy	nleg	R
Pb–O	100	12	2	2.84
Pb–Ti	27	5	2	3.48
Pb–Zr	18	3	2	3.48

Table 4.
Interatomic distances (R) and quality factor (QF) of the PBZT50 sample obtained through Pb L_{III}-edge filtered EXAFS fitting by tetragonal and cubic models.

		PBZT50			
Symmetry	**i**	**Shell**	**N_i**	**R (Å)**	**QF**
Tetragonal	1	Pb–O_I	4	2.54(1)	0.33
	2	Pb–O_{II}	4	2.88(2)	
	3	Pb–O_{III}	4	3.29(2)	
	4	Pb–Ti_I	3	3.33(2)	
	5	Pb–Zr_I	1	3.41(7)	
	6	Pb–Ti_{II}	2	3.67(4)	
	7	Pb–Zr_{II}	2	3.65(5)	
Cubic	1	Pb–O_I	12	2.87(5)	11.58
	2	Pb–Ti_I	5	3.52(1)	
	3	Pb–Zr_I	3	3.52(1)	

symmetry. Therefore, this qualitative analysis indicates even in a relaxor sample of a cubic long-range order structure, the Pb atoms show a significant degree of local distortion.

In summary, XRD, which provides information about the average structure at long-range distances, showed the structure of the PZT and PBZT samples exhibits a cubic symmetry at specific temperatures. On the other hand, XAS, which probes the short-range structure around the absorber atom, shows their local structure exhibits a tetragonal symmetry more compatible with the dielectric properties, especially in the PBZT40 and PBZT50 samples characterized as relaxors [24].

The different local symmetry observed by XRD and XAS has

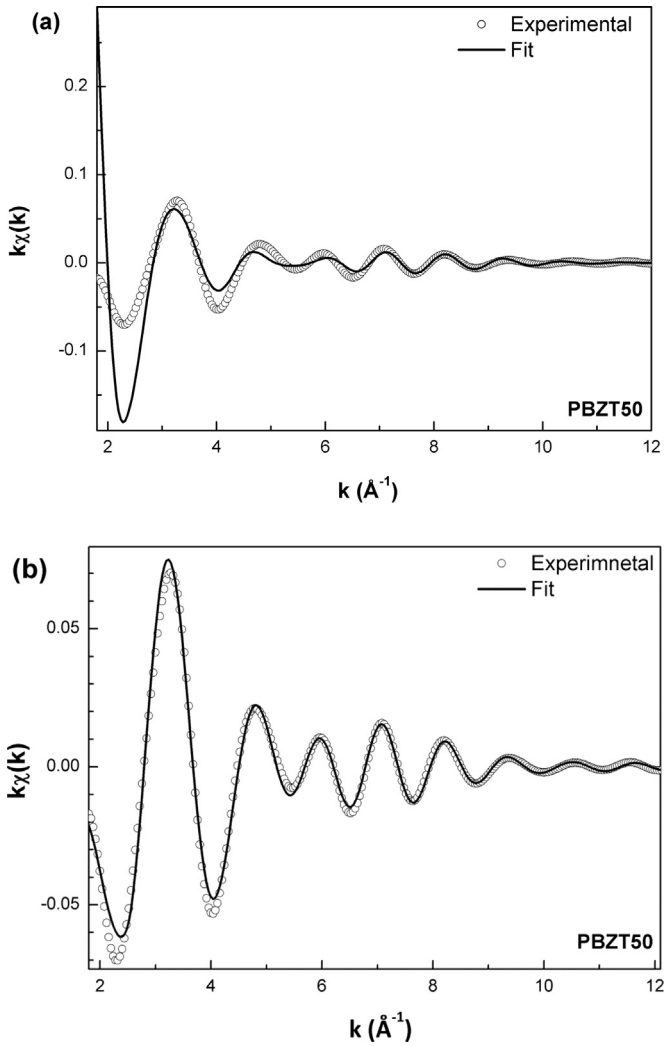

Fig. 4. Experimental and fitted back-Fourier-filtered for the PBZT50 sample at room temperature: (a) cubic and (b) tetragonal local symmetry models.

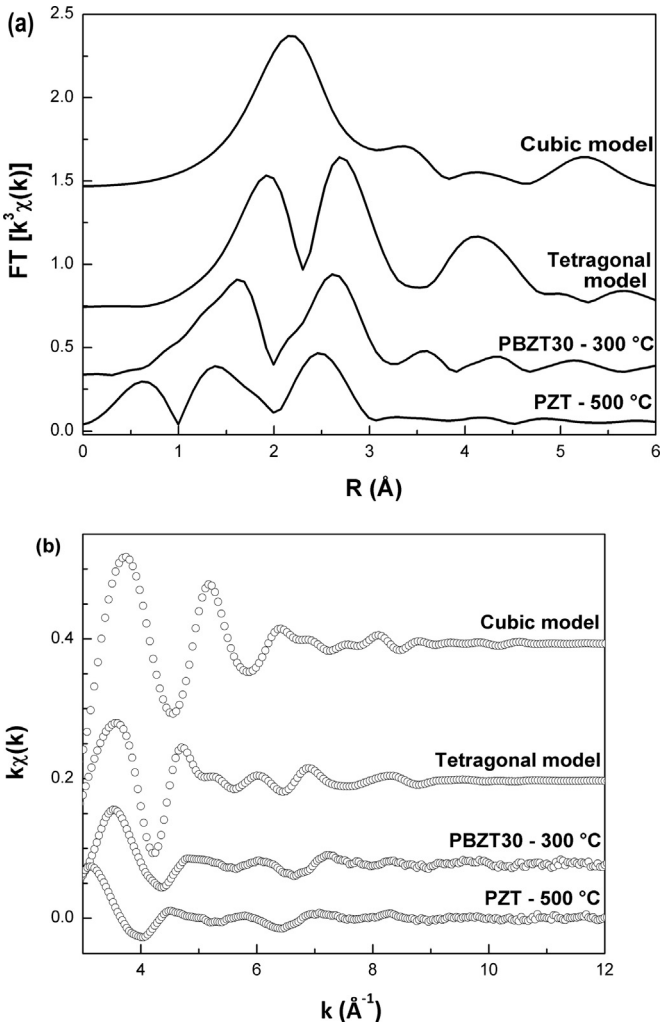

Fig. 5. Fourier transforms of PZT and PBZT30 at 500 °C and 300 °C, respectively.

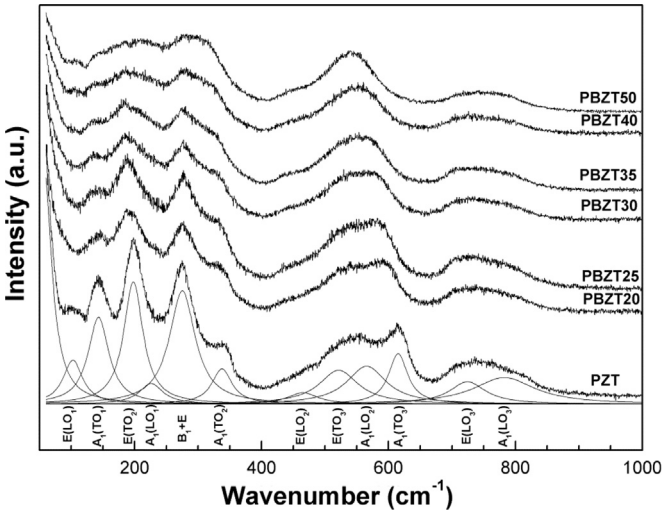

Fig. 6. Raman spectra of PBZT samples at room temperature.

also been reported by different authors [35–37]. By studying the $PbTiO_3$ compound at different temperatures, Sicron et al. showed Ti atoms are shifted from their ideal position above the Curie temperature whereas, according to XRD data, they occupy the ideal position in the TiO_6 octahedron [35]. Teslic and Egami also reported a discrepancy between local and long-range order structures when they studied $PbZr_{1-x}Ti_xO_3$, $Pb(Mg_{1/3}Nb_{2/3})O_3$ and $Pb_{1-x}La_xZr_yTi_{1-y}O_3$ systems through X-ray diffraction and neutron scattering measurements [36,37]. Their structural studies yielded evidence of slight local deviations from crystallographic lattice periodicity and local chemical ordering [36,37].

The apparent discrepancy between XAS and XRD results is related to the ability of the XAS technique to detect a local disorder in a perfectly long-range ordered structure. In XAS, the physical process involved in the absorption is of the order of 10^{-15} s, which is shorter than the time scale of the structural modifications that occur in the system and enable a dynamic and fast disorder process to be observed [35]. Regarding the X-ray diffraction technique, as local disorder cannot be detected, it is not considered in the structural model assumed [12]. Consequently, the XAS technique provides a better visualization of a local disorder than X-ray diffraction.

Fig. 6 shows the Raman modes of PBZT samples collected at room temperature indexed according to the spectrum of the $PbTiO_3$ tetragonal sample [38]. The XRD measurements showed all samples exhibit a tetragonal symmetry at room temperature, except the PBZT50 sample, which displays a cubic symmetry [39]. As the concentration of Ba atoms increases, the intensity of some modes decreases and frequency changes are also observed. The Raman spectra of the PBZT50 sample, characterized as cubic by XRD, show detectable bands of lower intensity in comparison with

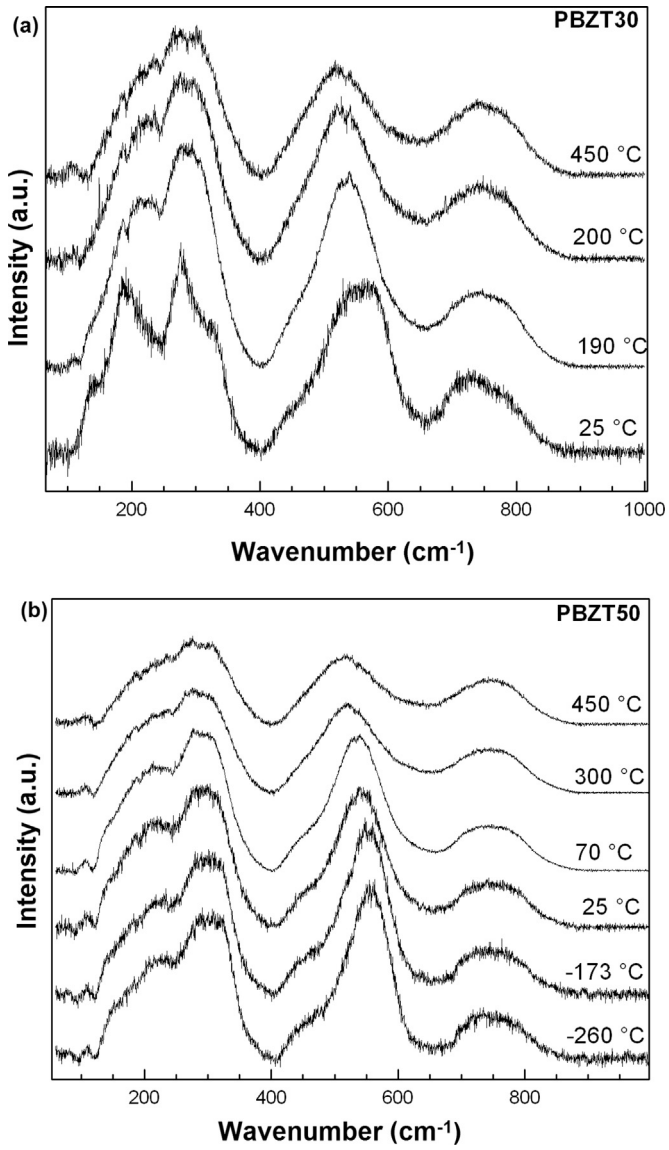

Fig. 7. Raman spectra as a function of temperature for: (a) PBZT30 and (b) PBZT50 samples.

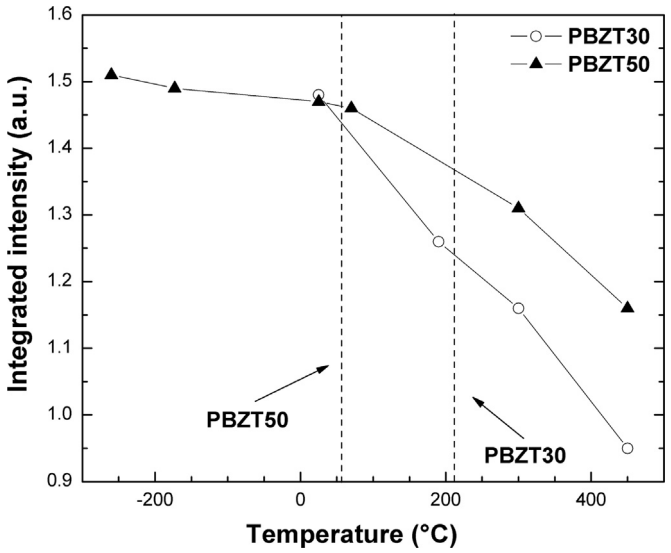

Fig. 8. Integrated intensity of $E(TO_3)$ mode as a function of temperature for PBZT30 and PBZT50 samples. Dashed lines correspond to T_m for each sample.

the other samples [39].

Fig. 7 shows the Raman spectra of PBZT30 and PBZT50 samples as a function of temperature. According to previous XRD results, the PBZT30 sample exhibits a cubic structure above 175 °C, whereas the PBZT50 sample exhibits a cubic structure at any temperature. As shown in Fig. 7, for both samples and independently of the long-range order symmetry or ferroelectric behavior, all Raman bands are detected at all temperatures.

According to selection rules, Raman bands are not expected in a perovskite cubic structure [40,41]. The presence of Raman modes in a long-range order cubic symmetry has been attributed to the displacement of Pb, Zr and Ti atoms from their center of symmetry [41]. According to Buixaderas et al. [41], if Zr and Ti atoms were off-center displaced from their octahedron in a long-range order cubic phase, at least seven and ten active modes would be observed in the infrared and Raman spectra, respectively. On the other hand, Itié et al. showed the displacement from the center of symmetry is not sufficient to justify the existence of Raman modes in a cubic phase and the anharmonicity terms of the vibrations on the lattice, which might induce a Raman activity should be considered [42].

Such Raman results are consistent with the results provided by the XAS technique, which showed a distorted local symmetry. El Marssi et al. attributed the presence of Raman modes in the cubic phase of PLZT samples to fluctuations in the polarization of the polar nanoregions [43]. However, as shown in Fig. 7, such modes are also observed in the Raman spectra of the PBZT30 sample at 450 °C, where the sample was characterized as paraelectric [24].

According to Fig. 7, the intensity of all Raman modes increases as the temperature decreases, except the modes between 400 and 600 cm^{-1}, which show a higher intensity increase. One of them, i.e, $E(TO_3)$, exhibits a particular behavior in relaxor ferroelectric perovskite samples in function of the temperature [43]. Fig. 8 shows the integrated intensity value of the $E(TO_3)$ mode of the PBZT30 and PBZT50 samples as a function of temperature. The integrated intensity value of the $E(TO_3)$ mode of the PBZT30 sample, which exhibits a normal ferroelectric behavior, varies linearly with the temperature, even below T_m (216 °C). For the PBZT50 sample, which exhibits a relaxor behavior, as the temperature decreases, the integrated intensity of the $E(TO3)$ mode increases up to a certain value and remains practically constant below T_m (56 °C). This behavior shows the process of correlation between nanodomains in a relaxor sample stabilizes at temperatures lower than T_m, which is in good agreement with the literature [43].

4. Conclusions

The local structure of the $Pb_{1-x}Ba_xZr_{0.40}Ti_{0.60}O_3$ system was characterized by Zr K-edge and Pb L_{III}-edge XAS and Raman spectroscopy.

The displacement of Zr atoms from the center of ZrO_6 octahedrons determined by EXAFS measurements is slightly influenced by the substitution of Pb^{2+} by Ba^{2+}. The local structure around Pb atoms at room temperature and temperatures above T_m is also distorted and incompatible with the local cubic symmetry determined by XRD. Therefore, this analysis indicates even in a relaxor sample of a cubic long-range order structure, that Pb atoms show a significant degree of local distortion. XAS, which probes the short-range structure around the absorber atom, shows that their local structure exhibits a tetragonal symmetry more compatible with the dielectric properties, especially in the samples characterized as relaxors.

The Raman modes in samples that exhibited a long-range order cubic symmetry confirmed the existence of a local disorder detected by XAS. The non variation of the integrated intensity of the $E(TO_3)$ mode of the PBZT50 sample showed the correlation between nanodomains, responsible for the relaxor phenomena, stabilizing below T_m. On the other hand, the intensity of this mode in PBZT30, characterized as a normal ferroelectric sample, varies linearly with temperature.

Acknowledgements

The authors are grateful to Brazilian funding agencies FAPESP (07/00011-1) and Capes (Grant no. BEX 2954/08-7). This research was partially conducted at LNLS (proposal XAFS1 - 13629) (Brazil) and SOLEIL (France) synchrotron facilities. The storage ring operators and EXAFS beamline scientists (S. Belin, V. Briois, E. Fonda from Soleil and A.P.S. Sotero and J.C. Maurício from LNLS) are highly acknowledged.

References

[1] Y. Xu, Ferroelectrics Materials and Their Applications, Elsevier Science Publishers B.V., Amsterdan, 1991.
[2] B. Jaffe, W.R. Cook, H. Jaffe, Piezoelectric Ceramics, Academic Press, London and New York, 1971.
[3] J. Frantti, S. Ivanov, S. Eriksson, H. Rundlof, V. Lantto, J. Lappalainen, M. Kakihana, Phase transitions of $Pb(Zr_xTi_{1-x})O_3$ ceramics, Phys. Rev. B 66 (2002) 064108.
[4] B. Noheda, D.E. Cox, G. Shirane, R. Guo, B. Jones, L.E. Cross, Stability of the monoclinic phase in the ferroelectric perovskite $PbZr_{1-x}Ti_xO_3$, Phys. Rev. B 63 (2001) 014103.
[5] M.H. Lente, E.N. Moreira, D. Garcia, J.A. Eiras, P.P. Neves, A.C. Doriguetto, V. R. Mastelaro, Y.P. Mascarenhas, Induction of relaxor state in ordinary ferroelectrics by isovalent ion substitution: a pretransitional martensitic texture case, Phys. Rev. B 73 (2006) 054106.
[6] L. Kozielski, M. Adamczyk, A. Lisinska-Czekaj, T. Orkisz, M. Piechowiak, D. Czekaj, Structure and dielectric properties of PZT-type ceramics with the diffuse phase transition, Phase Transit. 79 (2006) 427–433.
[7] T. Ikeda, Studies on (Ba–Pb)(Ti–Zr)O_3 system, J. Phys. Soc. Jpn. 14 (1959) 168–174.
[8] G. Li, G. Heartling, Dielectric, ferroelectric and electric field-induced strain properties of $(Pb_{1-x}Ba_x)(Zr_{1-y}Ti_y)O_3$ ceramics, Ferroelectrics 166 (1995) 31–45.
[9] S. Sharma, R. Singh, T.C. Goel, S. Chandra, Synthesis, structural and electrical properties of La modified PZT system, Comp. Mater. Sci. 37 (2006) 86–89.
[10] G.A. Samara, Ferroelectricity Revisited – Advances in Materials and Physics, Academic, New York, 2001.
[11] H.R. Favarim, A. Michalowicz, J.C. M'Peko, V.R. Mastelaro, Phase-transition studies of $Ba_{0.90}Ca_{0.10}(Ti_{1-x}Zr_x)O_3$ ferroelectric ceramic compounds, Phys. Status Solidi A 207 (2010) 2570–2577.
[12] P.P. Neves, A.C. Doriguetto, V.R. Mastelaro, L.P. Lopes, Y.P. Mascarenhas, A. Michalowicz, J.A. Eiras, XAS and XRD structural characterization of lanthanum-modified $PbTiO_3$ ceramic materials, J. Phys. Chem. B 108 (2004) 14840–14849.
[13] B. Ravel, E.A. Stern, R.I. Vedrinskii, V. Kraizman, Local structure and the phase transitions of $BaTiO_3$, Ferroelectrics 206 (1998) 407–430.
[14] V.A. Shuvaeva, D. Zekria, A.M. Glazer, Q. Jiang, S.M. Weber, P. Bhattacharya, P. A. Thomas, Local structure of the lead-free relaxor ferroelectric $(K_xNa_{1-x})_{(0.5)}Bi_{0.5}TiO_3$, Phys. Rev. B 71 (2005) 174114.
[15] V.A. Shuvaeva, I. Pirog, Y. Azuma, K. Yagi, K. Sakaue, H. Terauchi, I.P. Raevskii, K. Zhuchkov, M.Y. Antipin, The local structure of mixed-ion perovskites, J. Phys. Condens. Mat. 15 (2003) 2413–2421.
[16] V.A. Shuvaeva, D. Zekria, A.M. Glazer, Q. Jiang, S.M. Weber, P. Bhattacharya, P. A. Thomas, Local structure of the lead-free relaxor ferroelectric $(K_xNa_{1-x})_{(0.5)}Bi_{0.5}TiO_3$, Phys. Rev. B 71 (2005).
[17] S.J.L. Billinge, M.G. Kanatzidis, Beyond crystallography: the study of disorder, nanocrystallinity and crystallographically challenged materials with pair distribution functions, Chem. Commun. (2004) 749–760.
[18] A. Al-Zein, G. Fraysse, J. Rouquette, P. Papet, J. Haines, B. Hehlen, C. Levelut, G. Aquilanti, Y. Joly, Zr-shift at the origin of the exceptional piezoelectric properties of $PbZr_{0.52}Ti_{0.48}O_3$, Phys. Rev. B 81 (2010) 174110.
[19] C. Laulhe, F. Hippert, J. Kreisel, M. Maglione, A. Simon, J.L. Hazemann, V. Nassif, EXAFS study of lead-free relaxor ferroelectric $BaTi_{1-x}Zr_xO_3$ at the ZrK edge, Phys. Rev. B 74 (2006) 014106.
[20] I. Grinberg, P. Juhas, P.K. Davies, A.M. Rappe, Relationship between local structure and relaxor behavior in perovskite oxides, Phys. Rev. Lett. 99 (2007) 267603.
[21] I. Grinberg, A.M. Rappe, Local structure and macroscopic properties in $PbMg_{1/3}Nb_{2/3}O_3$–$PbTiO_3$ and $PbZn_{1/3}Nb_{2/3}O_3$-$PbTiO_3$ solid solutions, Phys. Rev. B 70 (2004) 220101.
[22] G.A. Samara, Pressure-induced crossover from long-to short-range order in compositionally disordered soft mode ferroelectrics, Phys. Rev. Lett. 77 (1996) 314–317.
[23] A. Mesquita, A. Michalowicz, V.R. Mastelaro, XANES measurements probing the local order and electronic structure of $Pb_{1-x}Ba_xZr_{0.40}Ti_{0.60}O_3$ ferroelectric materials, J. Alloy. Compd. 640 (2015) 355–361.
[24] A. Mesquita, A. Michalowicz, V.R. Masrelaro, Influence of Ba-substitution on the structural and ferroelectric properties of $Pb_{1-x}Ba_xZr_{0.40}Ti_{0.60}O_3$ ceramic materials, Phase Transit. 85 (2012) 659–674.
[25] A. Michalowicz, J. Moscovici, D. Muller-Bouvet, K. Provost, MAX: multiplatform applications for XAFS, J. Phys. Conf. Ser. 190 (2009) 012034.
[26] A.L. Ankudinov, B. Ravel, S.D. Conradson, J.J. Rehr, Real-space multiple-scattering calculation and interpretation of x-ray-absorption near-edge structure, Phys. Rev. B 58 (1998) 7565.
[27] ⟨http://ixs.iit.edu/subcommittee_reports/sc/⟩, IXS Standards and Criteria Subcommittee Reports, International XAFS Society, 2000.
[28] G. Mountjoy, D.M. Pickup, R. Anderson, G.W. Wallidge, M.A. Holland, R. J. Newport, M.E. Smith, Changes in the Zr environment in zirconia-silica xerogels with composition and heat treatment as revealed by ZrK-edge XANES and EXAFS, Phys. Chem. Chem. Phys. 2 (2000) 2455–2460.
[29] P.E.R. Blanchard, R.G. Cavell, A. Mar, Electronic structure of ZrCuSiAs and ZrCuSiP by X-ray photoelectron and absorption spectroscopy, J. Solid State Chem. 183 (2010) 1536–1544.
[30] A. Michalowicz, G. Vlaic, Multiple solutions in data fitting: a trap in EXAFS structural analysis and some ideas to avoid it, J. Synchrotron Radiat. 5 (1998) 1317–1320.
[31] S.D. Kelly, B. Ravel, EXAFS analysis with self-consistent atomic potentials, in: B. Hedman, P. Painetta (Eds.), X-Ray Absorption Fine Structure-Xafs13, 2007, pp. 135–137.
[32] D. Cao, I.K. Jeong, R.H. Heffner, T. Darling, J.K. Lee, F. Bridges, J.S. Park, K. S. Hong, Local structure study of the off-center displacement of Ti and Zr across the morphotropic phase boundary of $PbZr_{1-x}Ti_xO_3$ (x=0.40,0.47,0.49,0.55), Phys. Rev. B 70 (2004) 224102.
[33] I. Grinberg, V.R. Cooper, A.M. Rappe, Relationship between local structure and phase transitions of a disordered solid solution, Nature 419 (2002) 909–911.
[34] J.A. Rodriguez, A. Etxeberria, L. Gonzalez, A. Maiti, Structural and electronic properties of $PbTiO_3$, $PbZrO_3$, and $PbZr_{0.5}Ti_{0.5}O_3$: first-principles density-functional studies, J. Chem. Phys. 117 (2002) 2699–2709.
[35] N. Sicron, B. Ravel, Y. Yacoby, E.A. Stern, F. Dogan, J.J. Rehr, Nature of the ferroelectric phase transition in $PbTiO_3$, Phys. Rev. B 50 (1994) 13168–13180.
[36] S. Teslic, T. Egami, D. Viehland, J. Phys. Chem. Solids 57 (1996) 1537.
[37] T. Egami, S. Teslic, W. Dmowski, D. Viehland, S. Vakhrushev, Local atomic structure of relaxor ferroelectric solids determined by pulsed neutron and X-ray scattering, Ferroelectrics 199 (1997) 103–113.
[38] J. Frantti, V. Lantto, S. Nishio, M. Kakihana, Effect of A- and B-cation substitutions on the phase stability of $PbTiO_3$ ceramics, Phys. Rev. B 59 (1999) 12–15.
[39] A. Mesquita, V.R. Mastelaro, A. Michalowicz, In situ X-ray diffraction studies of phase transition in $Pb_{1-x}La_xZr_{0.40}Ti_{0.60}O_3$ ferroelectric ceramics, Phase Transit. 83 (2010) 251–262.
[40] Y. Ikeuchi, S. Kojima, T. Yamamoto, Raman scattering study of cubic to tetragonal phase transitions of Ti-rich $Pb(Zr_xTi_{1-x})O_3$, Jpn. J. Appl. Phys. 1 (36) (1997) 2985–2988.
[41] E. Buixaderas, I. Gregora, S. Kamba, J. Petzelt, M. Kosec, Raman spectroscopy and effective dielectric function in PLZT x/40/60, J. Phys. Condens. Mat. 20 (2008) 345229.
[42] J.P. Itie, B. Couzinet, A.M. Flank, P. Lagarde, A. Polian, High pressure XAS at the TiK edge on titanate perovskites, in: B. Hedman, P. Painetta (Eds.), X-Ray Absorption Fine Structure-XAFS13, American Institute of Physics, Melville, 2007, pp. 241–243.
[43] M. ElMarssi, R. Farhi, X. Dai, A. Morell, D. Viehland, A Raman scattering study of the ferroelectric ordering in rhombohedral and tetragonal La-modified lead zirconate titanate ceramics, J. Appl. Phys. 80 (1996) 1079–1084.